CDF note 7167

Search for New Physics with High Mass Tau Pairs in CDF

The CDF Collaboration
URL http://www-cdf.fnal.gov
(Dated: November 2, 2004)

We present the results of a search for new particles decaying to tau pairs, using data corresponding to integrated luminosity 195 pb^{-1} collected with the CDF detector of the Tevatron. Hypothetical particles, such as Z' and MSSM Higgs boson A can potentially produce such pairs. We discuss the methods of tau identification, and show the signal acceptance versus new particle mass. The low-mass region, dominated by $Z \to \tau\tau$, is used as a control region. No significant excess events over the estimated backgrounds is observed in the high-mass region, and we set upper limits on the cross section times branching ratio as a function of the Z' and A mass.

Preliminary Results for Summer 2004 Conferences

I. INTRODUCTION

This note describes a search for new physics with high-mass tau pairs in $p\bar{p}$ collisions at $\sqrt{s} = 1.96$ TeV with the CDF detector of the Fermilab Tevatron. Various new physics processes can lead to very high-mass tau pairs. Example signal processes include $Z' \to \tau\tau$ [1] and MSSM Higgs $A \to \tau\tau$ [2]. We use three final states with at least one hadronic tau decay: $\tau_e\tau_h$, $\tau_\mu\tau_h$ and $\tau_h\tau_h$ (Throughout this paper we use the short-hand notations τ_e, τ_μ and τ_h to denote $\tau \to e\nu\bar{\nu}$, $\tau \to \mu\nu\bar{\nu}$, and $\tau \to$ hadrons ν, respectively).

The main backgrounds are from the high-mass tail of $Z/\gamma^* \to \tau\tau$, and jet$\to \tau$ fakes from W+jets, di-jet, and multi-jet events. We define a mass-like quantity $m_{\rm vis}$ using the four-vectors of the lepton, the tau, and the $\not\!\!{\rm E}_{\rm T}$ vector (with z component set to zero, and energy equal to the magnitude of $\not\!\!{\rm E}_{\rm T}$). We perform a blind search in the region $m_{\rm vis} > 120\ {\rm GeV/c^2}$. The events in the region below this cut are used as control sample.

The CDF detector is described in detail in [3].

II. DATA SAMPLE & EVENT SELECTION

The study of $\tau_e\tau_h$ and $\tau_\mu\tau_h$ channels use data corresponding to an integrated luminosity of 195 pb^{-1}. The data was collected with a "lepton plus track" trigger, requiring an electron (muon) with ${\rm E_T}$ >8 GeV (${\rm p_T}$ >8 GeV/c) and an isolated track with ${\rm p_T}$ >5 GeV/c. From this sample we select events with a reconstructed isolated electron with ${\rm E_T} > 10\,{\rm GeV}$ (isolated muon with ${\rm p_T} > 10\ {\rm GeV/c}$), a reconstructed isolated tau with ${\rm p_T}$(seed track) >6 GeV/c and ${\rm p_T}$(tracks + π^0s) >25 GeV/c, and $\not\!\!{\rm E}_{\rm T}$ >15 GeV. The seed track is the highest ${\rm p_T}$ track in the tau candidate.

The $\tau_h\tau_h$ analysis uses data corresponding to an integrated luminosity of 72 pb^{-1} collected with the "tau plus $\not\!\!{\rm E}_{\rm T}$" trigger. It requires a tau candidate with ${\rm E_T}$ >20 GeV, and $\not\!\!{\rm E}_{\rm T} > 20$ GeV. From this sample we select events with $\not\!\!{\rm E}_{\rm T}$ >25 GeV and two isolated tau candidates with ${\rm p_T}$(seed track) >6 GeV/c. One of the taus must have ${\rm p_T}$(tracks + π^0s) >25 GeV/c and the second one ${\rm p_T}$(tracks + π^0s) >10 GeV/c.

A. Tau Identification

Tau identification at CDF proceeds by defining a tau signal and isolation cones around the tau seed track direction, shown in Figure 1. We require that there are no tracks or π^o's in the isolation annulus. The isolation cone is set to 30 degree (0.524 radian). We use a variable size ("shrinking") signal cone determined by the deposited energy by tau candidates. Figure 2 illustrates the function we use in the signal cone definition. The cone starts out at a constant 10 degree (0.175 radian), and then is defined by (5 radians)/$E_{\rm vis}$. To account for direction resolution, we set a low limit for the shrinking cone at 50 mradians. The shrinking signal cone, a natural consequence of the tau's relativistic boost, dramatically helps to reduce jet backgrounds in the high mass search.

B. Kinematic Cuts

We require that $\not\!\!{\rm E}_{\rm T}$ points within 30 degree of the direction of the electron (muon) for the $\tau_e\tau_h$ ($\tau_\mu\tau_h$) channel, or the lower-${\rm p_T}$ tau for the $\tau_h\tau_h$ channel. This cut retains most of the signal while significantly suppressing the backgrounds. In Figure 3 we use the $\tau_e\tau_h$ channel to illustrate the effect of the kinematic cuts on the signal and the dominant backgrounds.

C. Signal Acceptance and Background Estimate

The acceptance in the high-mass signal region is measured in a combination of data and Monte Carlo. We generate $f\,\bar{f} \to Z' \to \tau\tau$ and $gg \to A \to \tau\tau$ at $\tan\beta$=20 using the PYTHIA Monte Carlo generator [4]. The taus are decayed using the Tauola package [5]. Trigger efficiency is taken into account. The efficiency for identifying the isolated lepton (electron and muon) is scaled to the value measured in the data using the unbiased leg in Υ and Z^0 decays. The efficiency for identifying the isolated, high ${\rm p_T}$ hadronically decaying tau is scaled to the value measured in the data using $W \to \tau\nu$ events. The total acceptances as a function of mass are shown in Figure 4, for $f\,\bar{f} \to Z' \to \tau\tau$ and $gg \to A \to \tau\tau$, respectively.

After applying tau identification and kinematic cuts the dominant background is $Z/\gamma^* \to \tau\tau$. Other backgrounds come from jet$\to \tau$ fakes, $Z/\gamma^* \to ee$ and $Z/\gamma^* \to \mu\mu$. We use Monte Carlo simulation to estimate the contributions from the Drell-Yan processes. Instead of modeling all processes that could produce jet$\to \tau$ fakes, we estimate their contributions from the data using fake rates measured in the unbiased jet samples. The expected number of background events in the control region and signal region are summarized in Table II and Table III, respectively.

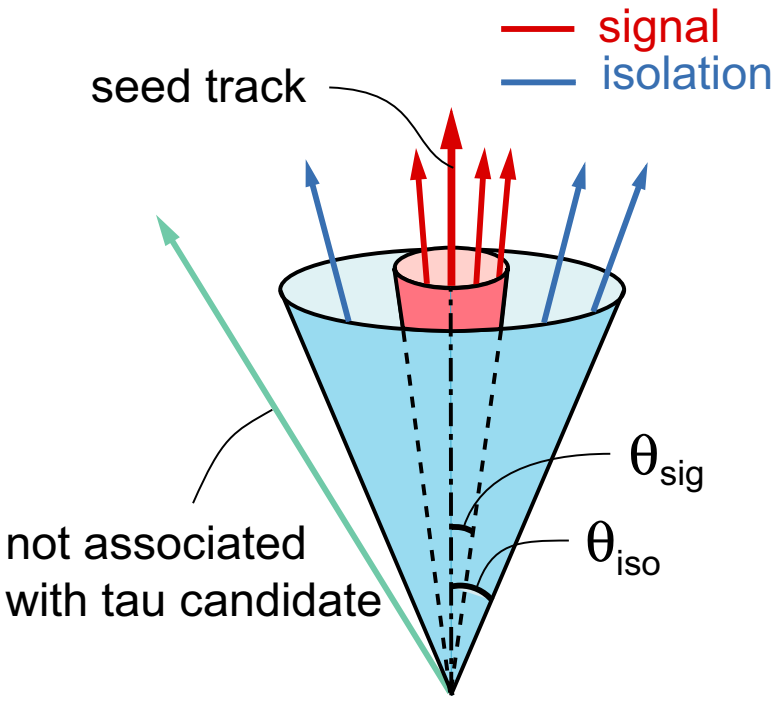

FIG. 1: Illustration of tau isolation cone definitions.

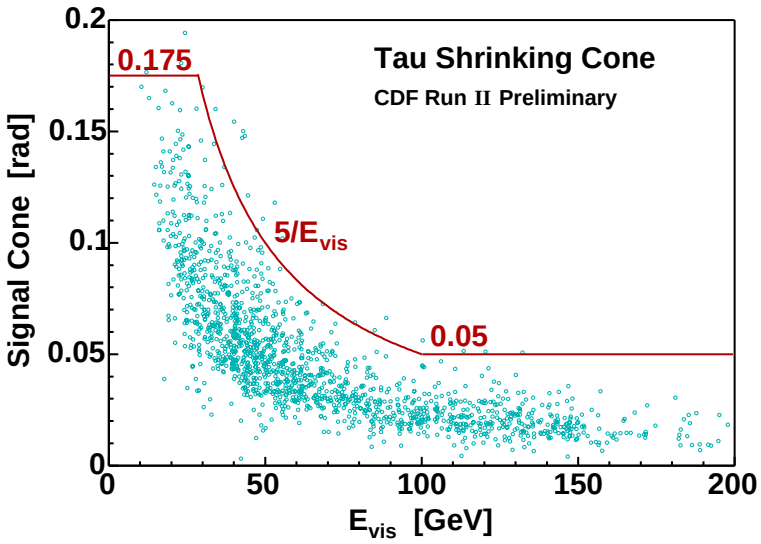

FIG. 2: Function used for the shrinking tau signal cone. We plot, at the generation level, the angle of additional tracks or π^os to the seed track as a function of visible tau energy.

III. SYSTEMATIC UNCERTAINTIES

Systematic uncertainties in this analysis come from Monte Carlo modeling of the signal acceptance, uncertainties on the Drell-Yan background estimates, and uncertainties on the jet$\rightarrow \tau$ fake background estimates.

The uncertainty on signal acceptance and the uncertainty on Drell-Yan background estimate include the contributions from Monte Carlo statistical uncertainty and trigger efficiencies (which are uncorrelated between channels), as well as the correlated errors listed below.

The jet$\rightarrow \tau$ fake background estimate itself reflects the effect of the average jet$\rightarrow \tau$ fake rate from events triggered on a

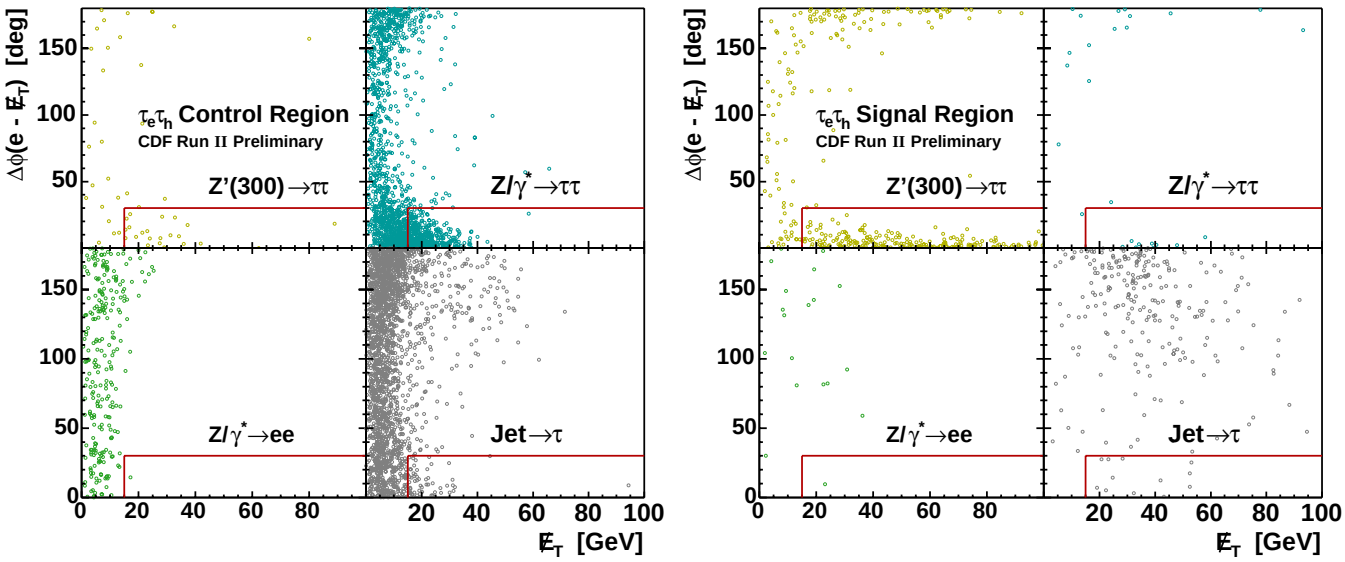

FIG. 3: Kinematic cuts $\not\!\!E_{\rm T}$ >15 GeV and $\Delta\phi(e - \not\!\!E_{\rm T}) < 30^{\rm o}$ for $\tau_e\tau_h$ analysis in (a) control region with $m_{\rm vis}$ <120 GeV/c^2 and (b) high-mass signal region with $m_{\rm vis}$ >120 GeV/c^2.

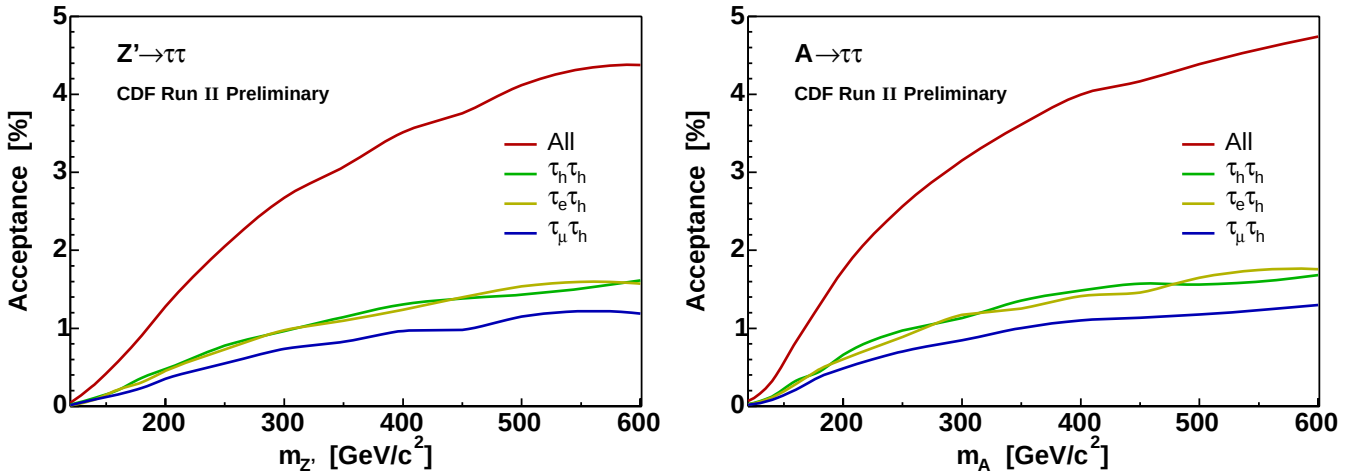

FIG. 4: Signal acceptance in the high-mass signal region as a function of mass for (a) $f\bar{f} \to Z' \to \tau\tau$ and (b) $gg \to A \to \tau\tau$.

jet with thresholds of 20, 50, 70 and 100 GeV. The uncertainty includes the contributions from statistical uncertainty and the systematic uncertainty due to jet$\to \tau$ fake rate which we take to be the biggest difference between the estimate using the average fake rate and the estimate using an individual fake rate.

Various systematic errors are correlated in various ways among the three channels. These include the effects of PDF, integrated luminosity, the lepton identification scale factors, $\not\!\!E_{\rm T}$, and jet$\to \tau$ fake rates. Table I lists the uncertainties and the nature of the correlations.

IV. RESULTS

Figure 5 shows the track multiplicity of hadronically decaying tau candidates in the control region. There is a strong enhancement in the one- and three-prong bins, resulting in a clear tau signature. This sample is dominated by $Z \to \tau\tau$ and there is small contribution from other backgrounds. A summary of the estimated backgrounds is presented in Table II.

After opening the box in the high-mass signal region, we observe 4 events in $\tau_e\tau_h$ channel, 0 event in $\tau_\mu\tau_h$, and 0 event in

	Uncertainty (%)	Applies to:
PDF	8	All channels
Luminosity	6	All channels
e ID scale factor	5	$\tau_e\tau_h$
μ ID scale factor	5	$\tau_\mu\tau_h$
τ ID scale factor	10	All channels
$\not\!\!E_{\rm T}$	6	All channels
Jet$\rightarrow\tau$ fake rate	20	All channels

TABLE I: Systematic uncertainties, in percent, and the affected channels.

Source	$\tau_e\tau_h$	$\tau_\mu\tau_h$	$\tau_h\tau_h$	Total
$Z/\gamma^* \rightarrow \tau\tau$	45.36±6.84	38.39±5.72	4.19±0.77	87.94±12.38
$Z/\gamma^* \rightarrow ee$	0.14±0.14	0	0	0.14± 0.14
$Z/\gamma^* \rightarrow \mu\mu$	0	0.48±0.25	0	0.48± 0.25
Jet$\rightarrow\tau$	3.83±1.03	3.72±0.88	3.16±0.55	10.71± 1.46
Total	49.32±6.94	42.59±5.85	7.35±0.95	99.27±12.55
Observed	46	36	8	90

TABLE II: The background summary and the observed in control region, 195 pb^{-1} (72 pb^{-1} for $\tau_h\tau_h$).

$\tau_h\tau_h$ channel. Table III shows a summary of the background estimates and the observed events. The $m_{\rm vis}$ distribution of the events in the control and signal samples is presented in Figure 6.

Since we observe no significant excess of events in the signal region, we set upper limits on the cross section times branching ratio as function of mass, using a Bayesian method. We calculated the 95% CL upper limits of $\sigma \cdot {\rm B}(f\bar{f} \rightarrow Z' \rightarrow \tau\tau)$ and $\sigma \cdot {\rm B}(gg \rightarrow A \rightarrow \tau\tau)$. We intend to use them as the generic limits for $\sigma \cdot {\rm B}(f\bar{f} \rightarrow X_{\rm vector} \rightarrow \tau\tau)$ and $\sigma \cdot {\rm B}(gg \rightarrow X_{\rm scalar} \rightarrow \tau\tau)$, which can be interpreted in various models. The results are shown in Figure 7.

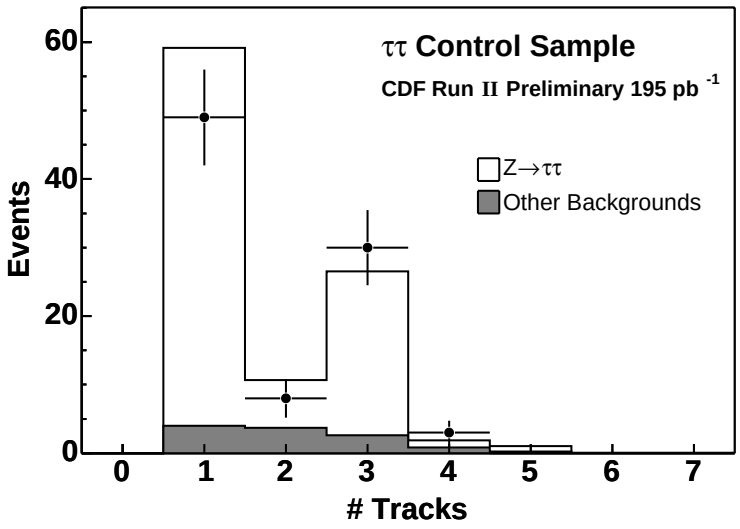

FIG. 5: Track multiplicity distribution for hadronically decaying tau candidates in the control region. The enhancements in the one- and three-prong bins show a clear tau signature.

Source	$\tau_e\tau_h$	$\tau_\mu\tau_h$	$\tau_h\tau_h$	Total
$Z/\gamma^* \to \tau\tau$	0.56±0.11	0.50±0.10	0.36±0.08	1.42±0.23
$Z/\gamma^* \to ee$	0.16±0.14	0	0	0.16±0.14
$Z/\gamma^* \to \mu\mu$	0	0.50±0.26	0	0.50±0.26
Jet$\to \tau$	0.29±0.14	0.18±0.09	0.28±0.10	0.75±0.19
Total Bkgd	1.01±0.24	1.18±0.30	0.64±0.13	2.83±0.46
Observed	4	0	0	4

TABLE III: Background estimates and observed events in the high-mass (signal) region, 195 pb^{-1} (72 pb^{-1} for $\tau_h\tau_h$).

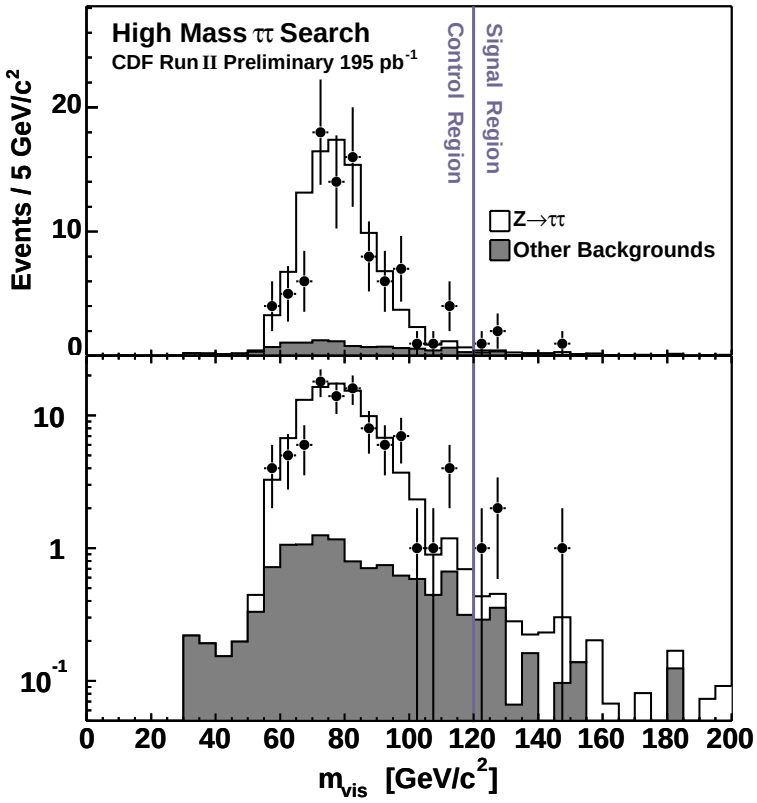

FIG. 6: Distribution of $m_{\rm vis}$ for the events in the control and signal region.

Acknowledgments

We thank the Fermilab staff and the technical staffs of the participating institutions for their vital contributions. This work was supported by the U.S. Department of Energy and National Science Foundation; the Italian Istituto Nazionale di Fisica Nucleare; the Ministry of Education, Culture, Sports, Science and Technology of Japan; the Natural Sciences and Engineering Research Council of Canada; the National Science Council of the Republic of China; the Swiss National Science Foundation; the A.P. Sloan Foundation; the Bundesministerium fuer Bildung und Forschung, Germany; the Korean Science and Engineering Foundation and the Korean Research Foundation; the Particle Physics and Astronomy Research Council and the Royal Society, UK; the Russian Foundation for Basic Research; the Comision Interministerial de Ciencia y Tecnologia, Spain; and in part by the European Community's Human Potential Programme under contract HPRN-CT-20002, Probe for New Physics.

[1] G. Altarelli, B. Mele and M. Ruiz-Altaba, Searching for new heavy vector bosons in $p\bar{p}$ colliders, Z.Phys. C45 (1989) 109.
[2] Report of the Tevatron Run 2 Higgs Working Group, eprint archive: hep-ph/0010338

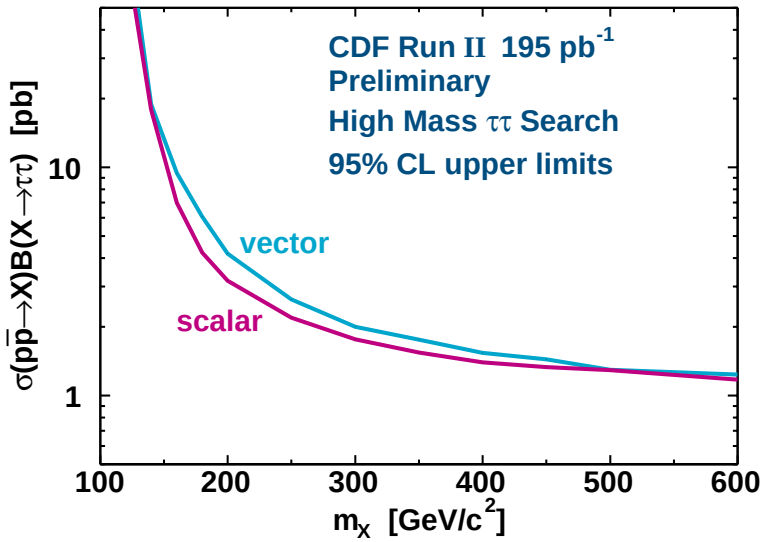

FIG. 7: The upper limits at 95% CL for $\sigma \cdot \mathrm{B}(f\bar{f} \to X_{\mathrm{vector}} \to \tau\tau)$ and $\sigma \cdot \mathrm{B}(gg \to X_{\mathrm{scalar}} \to \tau\tau)$.

[3] F. Abe, et al., Nucl. Instrum. Methods Phys. Res. A **271**, 387 (1988); D. Amidei, et al., Nucl. Instum. Methods Phys. Res. A **350**, 73 (1994); F. Abe, et al., Phys. Rev. D **52**, 4784 (1995); P. Azzi, et al., Nucl. Instrum. Methods Phys. Res. A **360**, 137 (1995); The CDFII Detector Technical Design Report, Fermilab-Pub-96/390-E

[4] T. Sjostrand et al., High-Energy-Physics Event Generation with PYTHIA 6.1, Comput. Phys. Commun. **135**, 238 (2001).

[5] S. Jadach, Z. Was and J.H. Kuehn, TAUOLA - A library of Monte Carlo programs to simulate decays of polarized leptons, Comp. Phys. Commun. **64** (1991).